Investigating Photoinduced Charge Transfer in Carbon Nanotube–Perylene–Quantum Dot Hybrid Nanocomposites

Joseph E. Weaver,[†] Mallika R. Dasari,[†] Aniket Datar,[†] Saikat Talapatra,[‡] and Punit Kohli[†,*]

[†]Department of Chemistry & Biochemistry and [‡]Department of Physics, Southern Illinois University, Carbondale, Illinois 62901, United States

ABSTRACT In this study, we investigate photophysical and photoinduced current responses of a nanocomposite which consists of multiwalled carbon nanotubes (CNTs), thiol derivative perylene compound (ETPTCDI), and cadmium selenide quantum dots (QDs). These QDs as well as the ETPTCDI harvest photons and transfer their excited electrons or holes to CNTs to complete the circuit. Both QDs and ETPTCDI contribute charges to the carbon nanotubes, which increased the overall photon harvest efficiency of the nanocomposite. Herein, we investigate through a series of photophysical photoluminescence quenching studies the charge transfer between donors (QDs and ETPTCDI) and acceptor (CNTs). The incorporation of ETPTCDI into the nanocomposite significantly increases the adhesion between QDs and CNTs through bonding between QDs and thiol groups on ETPTCDI and $\pi-\pi$ interactions between ETPTCDI and CNTs. Thus, ETPTCDI acted as a molecular linker between QDs and CNTs. Furthermore, a significant increase (>5 times) in the Stern–Volmer constant, K_{sv}, for QD emission after addition of ETPTCDI-tagged CNTs clearly indicates a large enhancement in the adhesion between CNTs and QDs. The nanocomposite shows a ~2–4-fold increase in the photoconductivity when exposed to AM1.5 solar-simulated light. The damage to the nanocomposite from the intensity of the solar-simulated light is also investigated. The proposed nanocomposite has the potential for photovoltaic applications such as being the active component in a hybrid bulk heterojunction solar cell.

KEYWORDS: carbon nanotubes · charge transfer · composite · nano · nanotechnology · nanocomposite · perylene · photoactive · photoconductive · quantum dots

Since the link between CO_2 and global climate change has been made,[1−3] the research and development as well as the production and storage of energy produced using alternative methods has significantly increased.[3−5] Photovoltaic (PV) solar cells are an excellent example of the production of alternative energy.[2,5,6] With oil prices on the rise and the risk for negative impact on the environment that on and off shore drilling has, the need to investigate alternative energy sources is imperative. The production of solar cells has increased significantly, driving down the cost of solar cell modules. Within the next decade, we can expect solar cell based energy production to be a significant contributor to the world's energy demand.[5,6] Currently, there are three generations of solar cells either on the market or in the research and development stage. The early solar cells consisted of doped monocrystalline silicon forming a p–n junction.[7] The efficiency for these solar cells is high (around 30–40%) but so is the price to fabricate them. Thin film solar cells were created to reduce the production cost and rival the early silicon films. Some common thin films used were cadmium telluride and copper indium–gallium diselenide (CIGS).[8] Third-generation solar cells are classified as either dye-sensitized (DSSC),[9] organic, and polymer solar cells.[10] These classifications are often blurred as researchers combine organic polymers and inorganic materials to form a "hybrid" solar cell.[11] Alivisatos's group has fabricated hybrid solar cells comprising CdSe nanocrystals or nanorods combined with organic donor poly(3-hexylthiophene) (P3HT), and when exposed to AM1.5 solar-simulated light, their device yielded a power conversion efficiency of 1–2%.[12−14] In general, all of these solar cells produce electron–hole pairs (excitons) that are bound by their coulomb attraction following photoexcitation. The separation of electrons and holes occurs at the donor–acceptor interface and transport to their corresponding electrodes, producing current in the external circuit.[15] In the late 1980s, organic based solar cells were reported with efficiencies near or at 1%.[16] Since then, researchers have developed organic solar cells with efficiencies up to 6%.[17] The most common organic polymer solar cell structure is the bulk heterojunction (BHJ) device in which an organic polymeric electron donor and electron acceptor are mixed into a solution and spin-cast as a thin

*Address correspondence to pkohli@chem.siu.edu.

Received for review August 11, 2010 and accepted October 03, 2010.

Published online October 14, 2010.
10.1021/nn1020067

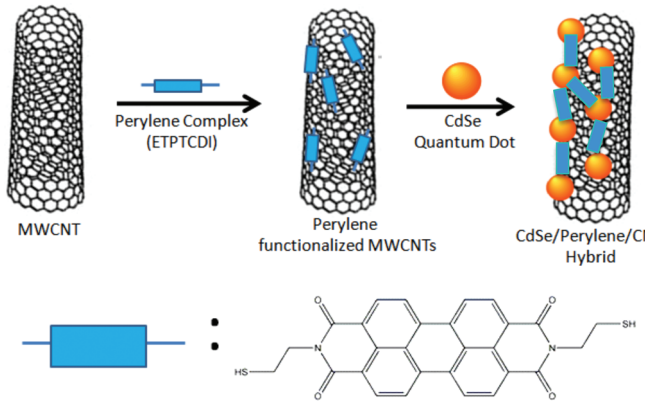

Figure 1. Schematic of nanocomposite assembly of QD−CNT−ETPTCDI used in these studies.

film that is placed between two electrodes, one electrode being optically transparent to allow light to pass into the BHJ active layer.[18] The first reported BHJ solar cell was published in 1995 and comprised a film of a poly(phenylene vinylene) (PPV) derivative blended with phenyl C_{61}-butyric acid methyl ester ($PC_{61}BM$). This particular BHJ solar cell relied on photoinduced charge separation that occurred as the PPV (donor) transferred electrons to the C_{61} (acceptor).[18,19]

CdSe quantum dots (QDs) are highly fluorescent semiconductor nanocrystals that exhibit size-dependent optical properties.[20,21] The quantum confinement effect of the QDs influences not only the optical properties but their electronic properties, as well.

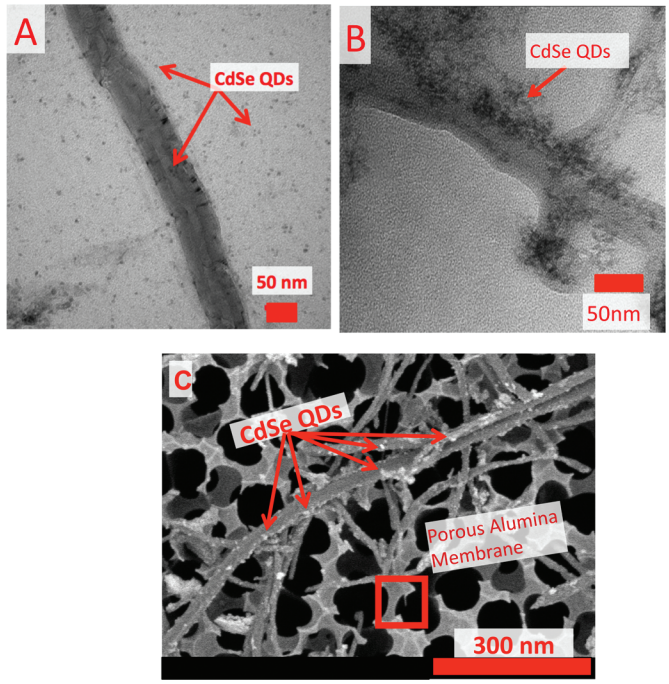

Figure 2. Transmission electron micrograph (TEM) of CdSe QDs adhered to CNTs through (A) van der Waals interactions, (B) ETPTCDI-functionalized CNTs. TEM electron beam intensity was 120 kV for all of the experiments. (C) High-resolution back-scattering field emission scanning electron microscopy (FE-SEM) image of QD−ETPTCDI−CNT nanostructures on porous alumina substrate. FE-SEM electron beam intensity was 1.0 kV.

As the size of the QD increases, the band gap decreases in energy until bulk material properties are obtained.[15,21] The tunable band gap, very large extinction coefficient, and high quantum efficiency make QDs an excellent candidate for a donor material. Carbon nanotubes (CNTs),[22] both single-wall and multiwalled carbon nanotubes, have become increasingly popular in the last two decades. CNTs have potential in several areas of interest including hydrogen storage, field emission devices, sensors/probes, and nanoelectronic devices.[23] The application of CNTs in conjunction with solar cell devices has become very popular in the photovoltaic (PV) field.[24] Conductive polymers and linker molecules have been combined with CNTs along with nanocrystals to produce hybrid organic solar cells.[25,26] CNTs have also been utilized as transparent electrode contacts for PV devices.[27] In recent studies, it has been shown that the addition of QDs to single-walled carbon nanotubes (SWNTs) resulted in the QDs adhering to the surfaces of the SWNTs through van der Waals interactions.[28] Recently, Juarez *et al.* demonstrated photocurrent production in a CNT−QD composite device.[29] Pyridine-protected CdSe nanocrystals have previously been synthesized to increase adhesion to single-walled carbon nanotubes through $\pi-\pi$ stacking of pyridine and carbon nanotubes.[30,31] Fabrication of a device in which the pyridine-capped CdSe nanocrystals are deposited between two microelectrodes shows a decrease in resistance as the device is exposed to various wavelengths of light.[31] In certain cases, rather than altering the chemistry of the CdSe QDs for adhesion to CNTs, the CNTs are functionalized with proper terminating functional groups that allow for increased adhesion to as-synthesized CdSe nanocrystals.[32] A more in-depth look into the charge transport properties between CdSe QDs and SWNTs was first analyzed by photophysical quenching in which excited state fluorescent QDs donate either an excited electron or hole to the SWNTs, thus resulting in the quenching of the QD photoluminescence (PL).[25] Flexible, lightweight polymer solar cell devices composed of poly(3-octylthiophene) (P3OT) embedded with CdSe−aminoethanethiol−SWNT hybrids have been previously reported. Upon solar-simulated illumination, the device was found to have an open-circuit voltage (V_{oc}) of 0.75 V.[33]

In this study, we investigate photocurrent response of a nanocomposite consisting of CNTs, ETPTCDI, and CdSe QDs. We also propose this nanocomposite as the active component in a PV solar cell. Here, ETPTCDI has two functions: first it acts as the linker molecule between the CdSe QDs and the CNTs. The terminal thiol functional group of our perylene derivative anchors itself through its strong affinity for CdSe QDs.[35] Second, ETPTCDI is a highly fluorescent molecule whose band gap energy levels match for efficient charge transfer to CNTs. Previous reports indicate that perylene is a prime

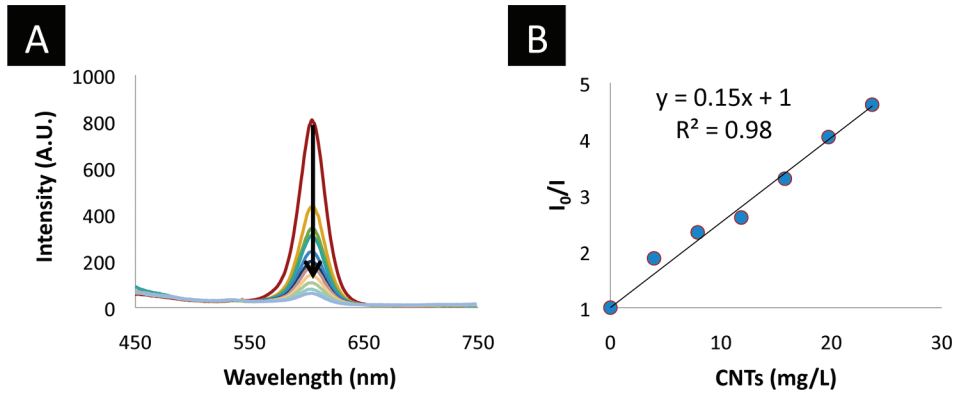

Figure 3. (A) Photoluminescence (PL) quenching of CdSe QDs with CNTs; 100 μL of 0.01% w/w CNTs in methanol was added to a solution of CdSe QDs (OD_{400nm} ~ 0.55) in chloroform placed in a quartz cuvette, which was followed by addition of 100 μL increments until a total volume of CNTs added was 1 mL. (B) Stern−Volmer plot of the quenching of CdSe QDs by the CNTs. The Stern−Volmer constant of QD quenching by CNTs was found to be K_{sv} = 0.15 L mg^{-1}. Excitation wavelength (λ_{ex}) was 400 nm. Slit width = 5.0 nm and scanning speed = 500 nm/min.

candidate for functionalizing CNTs.[34] The π-bonding bonds of perylene and CNTs allow for π−π stacking between perylene and CNTs.[25,34] Perylene based derivatives such as ETPTCDI have also been widely used as acceptor molecules in many organic based solar cells.[18] The results from this work show a good photoresponse to a solar simulator light source indicating the occurrence of the PV effect. Photophysical quenching studies further indicate the electron−hole transfer between the QDs and CNTs as well as the ETPTCDI and CNTs, making this system a good candidate for PV cells.

RESULTS AND DISCUSSION

QD−ETPTCDI−CNT Nanostructures. A schematic approach for the preparation of the nanocomposite is displayed in Figure 1. Initially, CdSe quantum dots were adhered to carbon nanotubes through van der Waals interactions. The sonication of a mixture of CdSe QDs and CNTs facilitated the adhesion process by breaking apart the CNT bundles, which increased the exposed CNTs' surface area to the QDs. A TEM image displays the CdSe QDs adhered to the CNTs (Figure 2A). The concentration of QDs attached to CNTs increased more than roughly 20 times following the functionalization of CNTs with ETPTCDI (Figure 2B,C). Viewing the two TEM images side by side indicates the effectiveness of functionalizing the CNTs with ETPTCDI. A TEM micrograph is, however, not a quantitative means to assess the electron transfer characteristic of the nanocomposite, but rather, it provides a direct evidence of increased adhesion of CdSe QDs to the CNTs. The morphology of the nanostructure was also visualized using a high-resolution field emission scanning electron microscope (Hitachi SU70) equipped with backscatter detection (Figure 2C). Back-scattered electrons (BSE) are electrons from the source electron beam that reflect off a sample through an elastic scattering mechanism. Elastic scattering is directly correlated to the material's elemental atomic number. Thus, a heavier atom displays a larger electron signal as compared to the signal originated for a lighter element.[40] In Figure 2C, the bright white crystals on the surface of the CNTs correspond to the CdSe QDs, clearly indicating enhanced adhesion of QDs onto CNTs.

PL Quenching Studies of CdSe QD−ETPTCDI−CNT Nanomaterials. ***PL Quenching of QD−CNT.*** PL quenching of CdSe and ETPTCDI with CNTs provides useful information on electron transfer between excited state CdSe or ETPTCDI and CNTs. CdSe QD PL was quenched as we injected a solution of 0.01% w/w CNTs in 100 μL increments (Figure 3A). The rate of PL quenching continued linearly until all of the QDs were essentially quenched. Stern−Volmer constants (K_{sv}) describe the accessibility QDs have to CNTs using the equation, $I_0/I = 1 + K_{sv}[CNT]$.[42] Higher K_{sv} provides a quantitative measure that the QDs are more accessible to the surface of CNTs. Table 1 summarizes the donor−acceptor pair K_{sv} values for all quenching experiments performed in our studies. A Stern−Volmer plot was created to quantify PL quenching of CdSe QDs by CNTs (Figure 3B). K_{sv} = 0.15 L/mg was determined for CdSe QDs adhered to CNTs, which is in agreement with K_{sv} of 0.18 L/mg for QDs quenched by amine-terminated CNTs.[42] These studies suggest that the interactions between QDs and CNTs are probably through van der Waals forces.

PL Quenching of ETPTCDI−CNTs. ETPTCDI quenching and Stern−Volmer curves are shown in Figure 4A,B, respectively. The K_{sv} value for the ETPTCDI−CNT pair was 1.3 L mg^{-1}. These experiments clearly suggested a strong

TABLE 1. Summary of K_{sv} Values for Each Donor−Acceptor Pair Investigated in Our Studies

PL molecule/particle (donor)	quencher (acceptor)	K_{sv}
QDs	CNTs	0.15 L mg^{-1}
ETPTCDI	CNTs	1.30 L mg^{-1}
QDs	ETPTCDI−CNTs	0.90 L mg^{-1}
QDs	ETPTCDI	0.31 μM^{-1}
ETPTCDI	QDs	minimal quenching observed
QDs	MPA	0.28 μM^{-1}

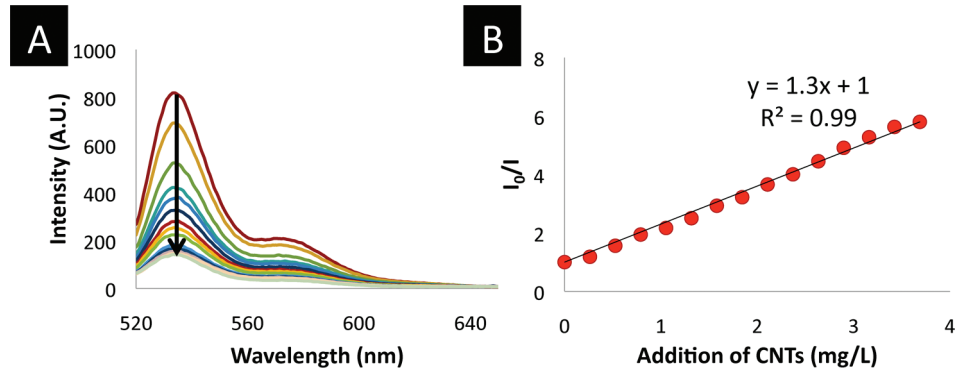

Figure 4. (A) PL quenching of ETPTCDI with addition of CNTs; 100 μL of 0.01% w/w CNTs in methanol was added to a 115 μM solution of ETPTCDI in methanol placed in a quartz cuvette and then in 10 μL increments. (B) Stern−Volmer plot of photophysical quenching of ETPTCDI by the addition of CNTs. The Stern−Volmer constant, K_{sv}, was found to be 1.30 L mg^{-1}. As a control experiment, the addition of a methanol equivalent to the largest volume in the previous experiment to the CNT solution did not produce any significant quenching. λ_{ex} = 490 nm, slit width = 5.0 nm, and scanning speed = 500 nm/min.

QD quenching by CNTs; this K_{sv} value for ETPTCDI photoluminescence quenching by CNTs was ~9 times larger than those for the QD−CNT system. This is reasonable because of strong π−π interactions between ETPTCDI and CNTs that resulted in strong adhesion and close proximity of ETPTCDI with CNTs. These conclusions are also consistent with the observed enhanced solubility of CNTs functionalized with ETPTCDI in a methanol solution.

PL Quenching of QD−ETPTCDI. Four experiments were performed to understand quenching of QDs (donor) with ETPTCDI (acceptor). Figure 5A,B shows UV−vis absorption and PL spectra, respectively, before and after addition of ETPTCDI to the QDs. The K_{sv} value for PL quenching of QDs with ETPTCDI was 0.31 μM^{-1}. The thiol functional group of the ETPTCDI is believed to play an important role in the quenching of the QDs. There are conflicting reports on the effect thiol functional groups have on the quantum yield of CdSe QDs.[43] Depending on the size and functional groups present, the thiol ligand can either stabilize the excited state charge and increase quantum yield or withdraw excited state electrons or holes quenching the QDs.[43] To understand the role the thiol ligand played in the quenching of QDs, we performed control PL quenching experiments in which 3-mercaptopropionic acid (MPA) was added to a solution of QDs. The thiol group of MPA forms a bond with QDs, and the PL quenching of MPA−QD studies provided important information on other possible quenching processes such as resonance energy transfer (RET) between ETPTCDI and QDs because MPA is not a chromophore and lacks any absorption spectral overlap with QD emission spectrum. Figure 5C displays the Stern−Volmer plot of QDs quenched by ETPTCDI (K_{sv} = 0.31 μM^{-1}) and also QDs quenched by MPA (K_{sv} = 0.28 μM^{-1}). Comparable K_{sv} values for ETPTCDI−QD and MPA−QD PL quenching studies suggested that the thiol−QD interaction played a dominant role in PL quenching of QDs and other quenching mechanisms such as RET had a minor role in the QD PL quenching. Thiol ligands are thought to quench QDs through a hole transport pathway in which the hole left behind from CdSe electronic excitation is transferred to the thiol ligand.[44] However, in our case, the presence of a π-bond network such as semiconducting perylene, the excited state electrons are more likely to be transferred from the QDs to ETPTCDI. The π-bonds within ETPTCDI are not only needed for adhesion to CNTs but also potentially act as a donor due to its HOMO/LUMO energy levels. The latter part will contribute to an increase in the photoresponse of the nanocomposite system.

In Figure 5D, the absorption spectrum of ETPTCDI is shown as CdSe QDs were added to the cuvette. It was observed that the ETPTCDI absorption spectrum began to start absorbing shorter wavelengths after the CdSe QDs were added, resembling the electronic absorption spectrum of CdSe QDs. On the basis of the calculated concentrations of QDs and ETPTCDI (2.3 and 1.3 μM, respectively, and extinction coefficients of 10^5 and 10^4 M^{-1} cm^{-1}, respectively), there was a significant amount of QDs present in the cuvette for interaction between QDs and ETPTCDI. Interestingly, Figure 5E displays the photoluminescence spectrum of the ETPTCDI as CdSe QDs were added, which shows minimal photoluminescence quenching after the addition of QDs to ETPTCDI. This observation along with large PL quenching of QDs by ETPTCDI suggests that electron transfer appears to occur from QDs to ETPTCDI because of a mismatch in the LUMO energy levels of ETPTCDI and QDs. Since the LUMO of ETPTCDI lies lower with respect to the conduction band of QDs, the excited electrons of ETPTCDI cannot be transferred to the LUMO of QDs (Figure 6). This is consistent with the absence of PL quenching of ETPTCDI after QD addition.

PL Quenching of QD−ETPTCDI−CNT. Photophysical quenching of QDs with ETPTCDI-functionalized CNTs was performed by injecting 0.01% CNT (w/w) in 10 μL increments to a QD solution (3.5 mL with OD_{400nm} = 0.55). Figure 7A depicts PL quenching data for this system. The K_{sv} value for the QD quenching by ETPTCDI−CNTs

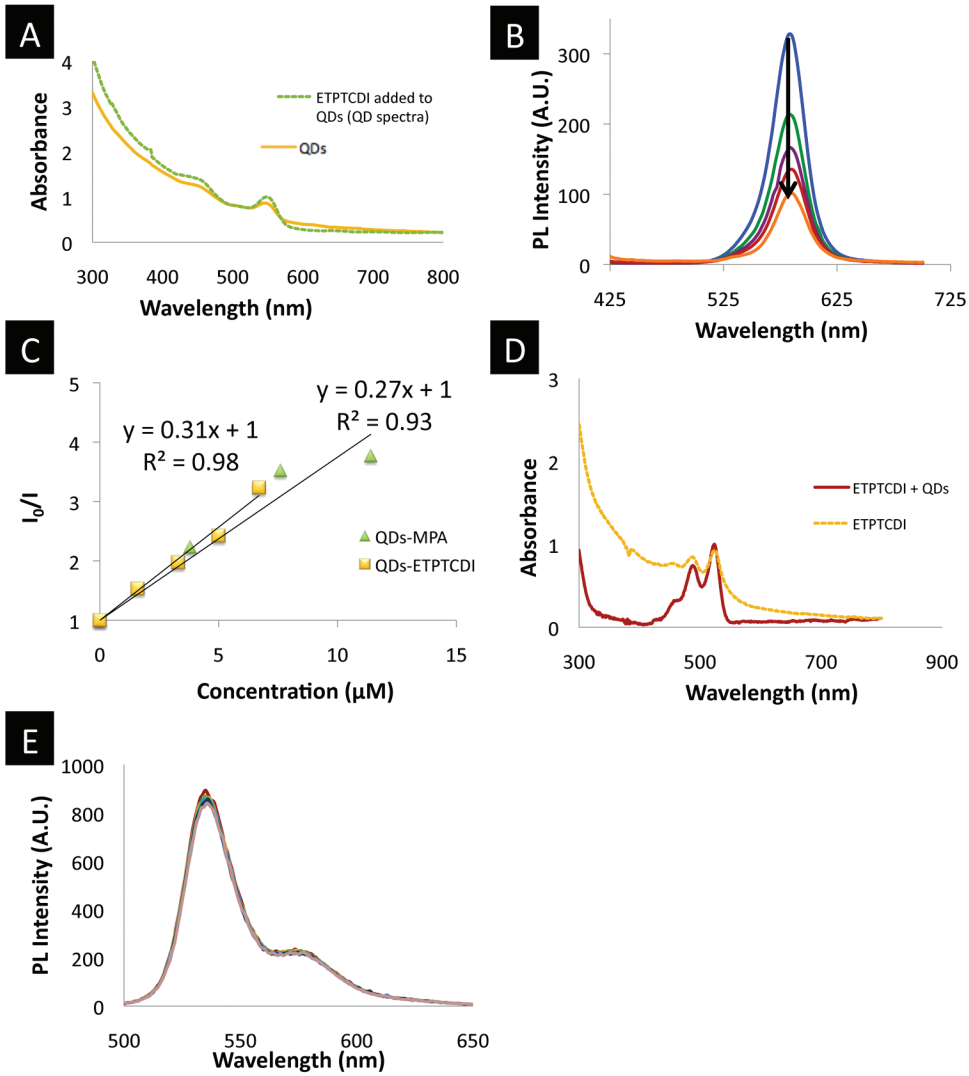

Figure 5. (A) Absorbance spectrum before and after the addition of 150 μL of ETPTCDI (5.0 mM) to 3.5 mL of CdSe QDs (OD_{400nm} = 1.50). (B) Photoluminescence quenching of 3.5 mL of CdSe QDs (OD_{400nm} = 0.50) by ETPTCDI (0.55 mM) in 50 μL increments (λ_{ex} = 400 nm, slit width = 5.0 nm, and scanning speed = 500 nm/min). (C) Stern−Volmer plots of QDs being quenched by ETPTCDI (K_{sv} = 0.31 μM^{-1}) and MPA (K_{sv} = 0.27 μM^{-1}); λ_{ex} = 400 nm, slit width = 5.0 nm, and scanning speed = 500 nm/min. (D) Absorbance spectrum before and after the addition of 150 μL of CdSe QDs (OD_{400nm} = 1.50) to 3.5 mL of ETPTCDI (5.0 mM). (E) Photoluminescence spectrum of 3.5 mL of ETPTCDI (5.0 mM) as 150 μL of CdSe QDs (OD_{400nm} = 1.50) was added (λ_{ex} = 490 nm, slit width = 5.0 nm, and scanning speed = 500 nm/min).

was 0.9 L mg^{-1} (Figure 7B), which lies between K_{sv} values for QD−CNT and ETPTCDI−CNT systems (Table 1).

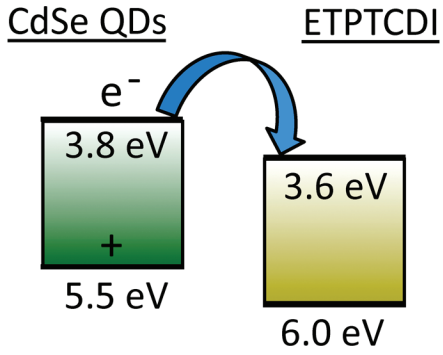

Figure 6. Electron transfer diagrams of CdSe QDs and ETPTCDI indicating that electron transfer occurs from QDs to ETPTCDI.

This is expected considering the very strong affinity for ETPTCDI and CNTs and a smaller affinity for QDs and CNTs. In fact, we designed ETPTCDI to contain two terminated thiol groups so that the CdSe QDs can anchor onto the ETPTCDI. The higher K_{sv} for QDs with ETPTCDI adhered onto CNTs appears to indicate a higher association of QDs adhered to thiol groups on CNTs than those without it. The K_{sv} for ETPTCDI−QDs was found to be higher than that for the QD−ETPTCDI−CNT system because free ETPTCDI molecules can potentially interact with two QDs, whereas ETPTCDI attached to CNTs leads to reduction in the degrees of freedom for ETPTCDI to interact efficiently with QDs. Overall, the enhanced adhesion of QDs with ETPTCDI-adhered CNTs is expected to facilitate the charge transfer processes between QDs and ETPTCDI (donors) and CNTs (accep-

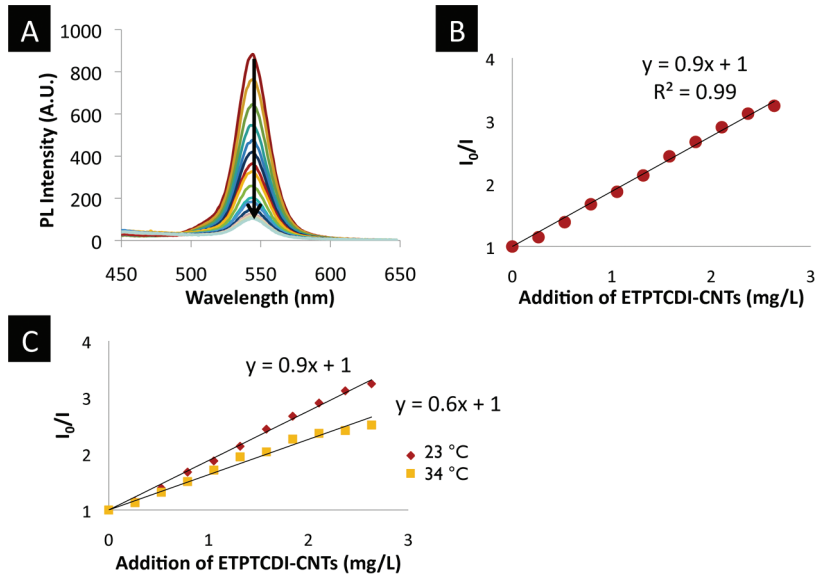

Figure 7. (A) PL quenching of QDs with the addition of ETPTCDI−CNTs (λ_{ex} = 400 nm); 100 μL of 0.01% w/w CNTs in methanol was added to a 115 μM solution of ETPTCDI in methanol placed in a quartz cuvette followed by 10 μL increments. (B) Stern−Volmer plot of photophysical quenching of QDs by the addition of ETPTCDI−CNTs. K_{sv} for this system was found to be 0.9 L mg^{-1}; λ_{ex} = 400 nm, slit width = 5.0 nm, and scanning speed = 500 nm/min. (C) Stern−Volmer plot of CdSe QDs being quenched by ETPTCDI−CNTs to determine the quenching mechanism. The Stern−Volmer constants, K_{sv}, for ambient temperature (23 °C) and 34 °C temperatures are 0.87 and 0.62 mg^{-1}, respectively; λ_{ex} = 400 nm, slit width = 5.0 nm, and scanning speed = 500 nm/min.

tors) and is expected to increase the PV efficiency of solar cell devices.

PL quenching, in general, is through one or more combinations of the following processes: static quenching, dynamic quenching, energy transfer, and charge transfer interactions. Static, dynamic and charge transfer require intimate or close contact between the donor and acceptors, whereas with dipole−dipole interactions between donor and acceptor can have energy transfer at a much larger distance (up to 10 nm).[45] In a previous study, PL quenching between QDs and CNTs was mainly attributed to dynamic quenching along with a component from an energy transfer mechanism.[24] In our case, we believe that the major PL quenching factor between the QDs and ETPTCDI-functionalized CNTs appears to be static quenching. An increase in temperature of the sample solution to 37 °C led to a smaller K_{sv} of 0.6 L mg^{-1} from 0.9 L mg^{-1} at 23 °C (Figure 7C). This observation suggests that QDs and ETPTCDI have relatively strong interactions in solution in their ground states. This is quite reasonable since ETPTCDI is strongly bonded to the CNTs in its ground state through π−π interactions and QDs can bond to ETPTCDI through a thiol bond. Thus, an increase in temperature of the sample solution led to decreased quenching (lower K_{sv}) because some of the ground state complexes [QD−ETPTCDI (donors) and CNTs (acceptors)] dissociate, resulting in an enhanced emission.

Photocurrent Response of Nanocomposite. In order to use this nanocomposite in PV applications, we investigated the light-harvesting photoconductive properties of the nanocomposite. A schematic diagram of the experimental setup for measuring the photocurrent generated in our QD−ETPTCDI−CNT composite is shown in Figure 8A. It is a two-electrode setup where QD−ETPTCDI−CNT nanocomposites were deposited (300−500 nm thickness measured using AFM) between the two gold electrodes. The photoinduced current was measured using a Keithley 6487 picoammeter while irradiating the nanocomposite with solar-simulated light. The light source is a 150 W xenon arc lamp with an AM1.5G filter (Newport Inc.). The intensity of the light at the device was found to be 300 mW/cm^2. Figure 8B shows a typical photocurrent−time plot while alternating between light and dark states for the nanocomposite deposited on glass substrates. The light source was shuttered at various times, reducing the amount of photogenerated current produced, as seen in Figure 8B. When exposed to solar-simulated light, the current increased ~10-fold as compared to the dark state (light is "off"). Figure S7 (Supporting Information) displays the linear ohmic response of the current as the voltage was swept from −10 V to +10 V, which shows ohmic response. This indicates that CNTs are dominant charge carriers in these devices (see below). The increase in the photocurrent with exposure to solar-simulated light indicates that there is a photoinduced charge generation process in our system. The photocurrent decreased over an extended period of time with numerous on−off light cycles probably due to photodamage to the active materials (Figure 8B). Following the deposition of fresh photoactive QD−ETPTCDI−CNT nanocomposites, the photogener-

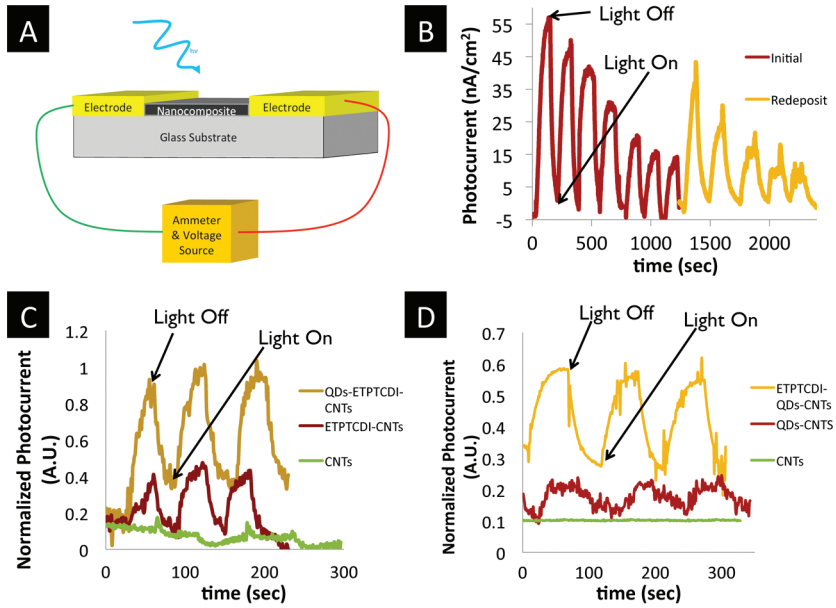

Figure 8. (A) Schematic representation of the device used in measuring the photocurrent generated from the nanocomposites. (B) Photogenerated current from QD−ETPTCDI−CNT nanocomposite device over time. The light source was a 150 W xenon arc lamp with an AM1.5 filter, and the measured intensity at the device was 300 mW/cm^2. The active area of the device was 15 mm × 80 μm. A secondary drop cast of nanocomposite was used to replenish the exhausted initial nanocomposite. All of the experiments were performed in ambient air. (C) On/off solar-simulated light cycles of photogenerated current *vs* time for ETPTCDI−CNTs (red) after addition of QDs (blue) to the same device. (D) On/off light cycles for QD−CNT (blue) device with addition of ETPTCDI (red). Green curves in panels C and D show the photocurrent−time response for devices consisting of only CNTs.

ated current was restored, supporting the argument of photoinduced damage to the active material during radiation. Without encapsulation of the device or with high/long intensity light exposure, we expected to have large photoinduced damage to the devices because upon illumination both QDs and ETPTCDI will be in their respective excited states and are highly reactive to surrounding molecules.

We have found that the adsorption of both ETPTCDI and QDs on CNTs showed photocurrent (Figure 8C). The addition of ETPTCDI to CNTs showed photocurrent response with time and proceeded to increase more than double with the addition of QDs to the ETPTCDI−CNTs to the same device. Similarly, the photocurrent for QD−CNTs was much smaller, but it increased >3 times with addition of ETPTCDI to the device (Figure 8D). The QD−CNT device was photoactive, but its response was lower than that of the ETPTCDI−CNTs. We believe this is due to the lack of affinity of CdSe QDs for CNTs without the thiol-terminated perylene derivative (ETPTCDI) which reduces the interaction between CNTs and QDs. Furthermore, the concentration of QDs on CNTs was also increased >20 times after ETPTCDI functionalization of CNTs. Two control devices consisting solely of ETPTCDI and the other of CdSe QDs were tested for photoconductivity. These devices yielded no significant photocurrent under the same experimental conditions. Furthermore, the photocurrent response of the nanocomposite consisting of QDs added to ETPTCDI−CNTs was much larger than the nanocomposite made up of QDs−CNTs with the later addition of ETPTCDI (Figure 8C,D). These experiments appear to suggest that the presence of ETPTCDI and QDs acts cooperatively for the enhancement of photoconductivity response of QD−ETPTCDI−CNTs (Figure 8D). Since both materials act as a donor to the system, their overall photocurrent was significantly larger than their individual photoresponse. These experiments also indicate that, although ETPTCDI and QDs interact intimately with CNTs, the use of two donors with different optical responses could be beneficial to the overall photocurrent characteristics of the solar cell.

We have also investigated the effect of temperature on the performance of the nanocomposite device. The high intensity light source of the solar simulator led to the production of heat at the interface of the nanocomposite. Initially, we used a steady flow of argon gas to cool the device down 10 °C. The cooling of the de-

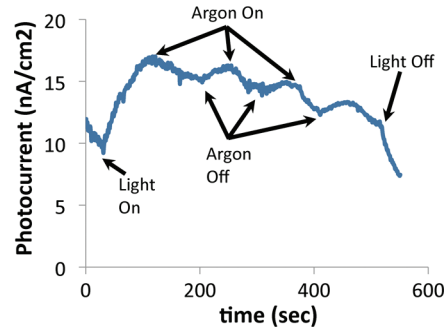

Figure 9. Change in photocurrent *versus* time under argon gas. The flow of argon gas led to a small decrease in the photocurrent.

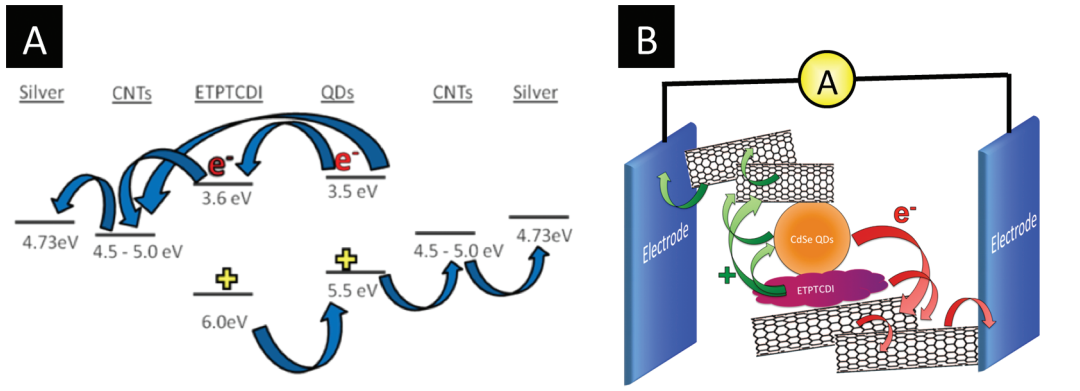

Figure 10. (A) Schematic of the energy diagram for different materials (QDs, ETPTCDI, and CNTs) present in the nanocomposite films. (B) Graphical representation of electron and hole transport paths within the nanocomposite. CNTs acted as electron acceptor and hole and electron transport conductors, as well.

vice leads to slightly lower photoinduced current values than without argon flow (Figure 9). A previous report displays similar photocurrent−temperature results and suggested that due to the electronic properties the photocurrent from a CNT mesh significantly increases as temperature increases and the photocurrent then decreases as the temperature returns to room temperature.[47] We attribute a slight reduction in photocurrent at a lower temperature to the slow energetic properties of the nanocomposite at a lower temperature.[46]

Now, the question is what are the electron and hole transport pathways that generate the observed current. The proposed nanocomposite contains two donors (QDs and ETPTCDI) and an acceptor (CNT). In our experiments, we believe that CNTs also acted as a charge transport conductor. In Figure 10A,B, a schematic representation provides the proposed flow of electron and hole in our nanocomposites and a graphical representation of our proposed electron−hole pathway of the nanocomposite. Since CNTs have the unique ability to transport both hole and electron, a fraction of CNTs transport electrons from QDs, ETPTCDI, or both in tandem to one electrode. Another fraction of CNTs transport holes to the other electrode that resulted in photogenerated current. Thus, our simple design with a nanocomposite between two metal electrodes showed photocurrent response without the use of materials that conduct electrons and holes separately as is commonly used in PV devices. This is also supported by a linear ohmic $I-V$ response (see below and Figure S7 in Supporting Information). However, we would also like to point out that, since both electrons and holes are transported through CNTs, these devices may have a lower PV efficiency as compared to those devices that contain separate media for holes and electrons. This is because some CNTs would carry electrons and holes at the same time, leading to recombination (waste of harvested excitons) and lowering of PV efficiency.

Lastly, we propose a possible bulk heterojunction (BHJ) hybrid solar cell based on this fabricated nanocomposite. Figure 11 displays a schematic representation of our proposed BHJ hybrid solar cell. The nanocomposite would be utilized as the active layer of the hybrid solar cell. Today's thin film solar cells are fabricated in a layered fashion and to prevent exciton recombination within the layers, conductive transparent polymer layers such as poly(3,4-ethylenedioxythiophene) and poly(styrenesulfonate) (PEDOT:PSS) are incorporated to enhance transport of holes to their proper electrode or anode.[48] Other polymers such as poly(3-hexylthiophene) (P3HT) can also be used to aid in the electron mobility of the exciton pairs to the electrodes.[49] Our future studies will be focused on the fabrication, characterization, and the optimization of solar cell devices utilizing QD−ETPTCDI−CNT nanocomposites.

CONCLUSION

In conclusion, we have fabricated a photoactive nanocomposite comprising CdSe QDs, a thiol based perylene (ETPTCDI), and multiwalled carbon nanotubes (CNTs). Our results on PL quenching and photoinduced current responses of each component within the nanocomposite show the charge transfer from ETPTCDI and QDs (donors) to CNTs (acceptors). Furthermore, CNTs also appear to act as an electron and hole transport

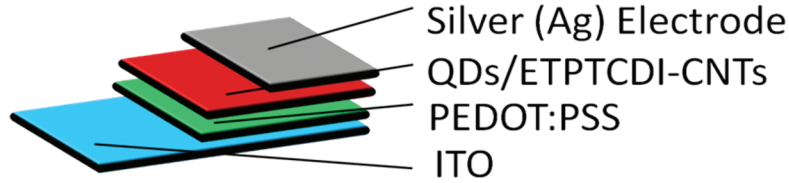

Figure 11. Schematic representation of proposed thin film heterojunction nanocomposite hybrid solar cell.

conductor. Alongside the use of TEM imaging, the PL quenching studies also indicate significant enhancement in the molecular interactions of QDs with CNTs. This photoactive nanocomposite has the potential of being an active layer for producing photocurrent in a hybrid BHJ solar cell.

EXPERIMENTAL SECTION

Materials. 2-Aminoethanethiol (~95%), tri-*n*-octylphosphine, and trioctylphosphine oxide (>90%) were all purchased from Sigma-Aldrich. Perylene-3,4,9,10-tetracarboxylic dianhydride (Fluka), ethanol (Decon Laboratories), and methanol (Fisher Scientific) were also used. Cadmium oxide (CdO), octadecylamine, selenium powder, and stearic acid were purchased from Acros Organics. Chloroform and dichloromethane were purchased from Mallinckrodt Chemicals. All chemicals were used as received without any further purification.

CdSe QDs Preparation. The synthesis of CdSe QDs was performed using a procedure from a previously published paper.[36,37] A typical synthesis is as follows: octadecylamine (2.05 g) was heated in a two neck 100 mL round-bottom flask to 150 °C for roughly 30 min to remove all water from octadecylamine. The flask was then allowed to cool to room temperature where CdO (13 mg), stearic acid (0.10 g), and tri-*n*-octylphosphine oxide (2.05 g) were combined in a two neck 100 mL round-bottom flask containing octadecylamine. The flask, equipped with a condenser, was sealed and placed under a continuous flow of argon. The flask was heated to 300 °C and rapidly stirred until the reddish-brown liquid became optically clear with a pale yellow color. At this time, a solution containing Se powder (79 mg) completely dissolved in trioctylphosphine (1 mL) was swiftly injected into the flask at 300 °C. Immediately following the injection, samples were extracted at intervals of 5−10 s. Each individual sample was placed in a test tube and allowed to cool to 25 °C, and PL of each sampled QD was visualized under a hand-held UV source (Figure S1). Approximately 1 mL of chloroform was added to each test tube to saturate the QDs from a dried solid state to a muddy liquid state. Next,the test tubes were filled with ethanol (~5 mL) and shaken vigorously to remove as much excess amine and TOPO as possible from the solution. Test tubes containing the QDs, ethanol, and chloroform were centrifuged at 14 000 rpm for 1−2 min. The hydrophobic QDs were precipitated out as pellets at the bottom of the test tubes, and the rest of the solution containing the excess amine, TOPO, ethanol,and chloroform was decanted off. QD precipitant was dispersed into 2−3 mL of fresh chloroform. In most cases, multiple purification steps were performed using the same procedure as described above. The final CdSe QD product was characterized using photoluminescence (PL) spectroscopy and UV−vis absorption spectroscopy (Figure S2A,B, respectively). Transmission electron microscopy (TEM) was also performed to visualize the QD morphology and size information (Figure S3).

Multiwalled Carbon Nanotube (CNT) Preparation. Vertically aligned CNTs were made using a method from a previously published article.[38,39] In brief, a ferrocene−xylene chemical vapor deposition (CVD) method was used for the growth of vertically aligned CNTs on Inconel substrates. A solution containing 1 g of ferrocene in 100 mL of xylene was injected into a tube furnace using a syringe pump at a pumping speed of <0.11 mL/min while the furnace containing the Inconel substrates was maintained at 790 °C. A mixture of 85% argon and 15% hydrogen was flown at 500 sccm to carry the xylene vapors containing the catalyst before entering the furnace. Figure S4A,B displays the SEM and TEM micrographs, respectively, of these synthesized CNTs.

Ethanethiol−Perylene Tetracarboxylic Diimide (ETPTCDI) Preparation. The synthesis of the ETPTCDI was performed according to a reported paper.[40] In a typical synthesis of ETPTCDI, perylene-3,4,9,10-tetracarboxylic dianhydride (PTCDA) (0.31 g), 2-aminoethanethiol (0.72 g), and imidazole (6.0 g) were all heated to 120 °C for 3 h under argon. The flask is then cooled to room temperature where 100 mL of ethanol and 300 mL of 3 M HCl were added and stirred overnight. The contents of the flask were then filtered over Whatman filter paper and refiltered until the eluent became clear. The filtrate was then washed with distilled water until the pH became neutral. ETPTCDI product was then dried under vacuum at 60 °C overnight. ETPTCDI was slightly soluble in DMSO, making it difficult to perform NMR characterization. ETPTCDI was, however, soluble in trifluoroacetic acid (TFA), but due to the very low pH of TFA, we could not use it in conjunction with QDs as TFA was found to significantly quench the PL of QDs. To visualize the fluorescence of the ETPTCDI solution, an optical image was taken to show its photoluminescence (Figure S5). The characteristic photoluminescence and absorbance are spectrally displayed as well in Figures S6A,B, respectively.

Adsorption of ETPTCDI on CNTs. A sample of CNTs (4 mg) was suspended in 50.0 mL of DMSO and subjected to sonication for 3 h to ensure that the majority of the CNT bundles were separated into individual carbon nanotubes. The CNT solution (0.01 wt %) was then stored for our studies. A 5.0 mL solution of ETPTCDI (~500 μM) was combined with 5.0 mL of the CNT stock solution to give an overall CNT concentration of 0.005% w/w. The solution was sonicated for approximately 1−2 h. ETPTCDI molecules were then allowed to fully adhere to CNTs as the solution was stored overnight in the dark. The combined solution was then filtered through a 200 nm porous alumina membrane (Whatman Anodisc) to remove excess ETPTCDI molecules (confirmed with UV−vis absorption spectroscopy). ETPTCDI-functionalized CNTs were then released from the Anodisc *via* sonication in DMSO for 1 h and diluted to a concentration of 0.01% w/w of ETPTCDI−CNTs in DMSO. The ETPTCDI−CNT composites were then stored in the dark for future use in the overall nanocomposite synthesis. The functionalization of CNTs with ETPTCDI significantly improved solubility in many organic solvents (methanol, ethanol, DMSO, chloroform, and dichloromethane).

Adhesion of QDs to ETPTCDI−CNTs. QDs on to ETPTCDI-functionalized CNTs were adhered by adding 5 mL of QDs with an OD_{400nm} of 0.45 to a vial containing 5 mL of the 0.01% w/w stock ETPTCDI−CNT solution. The combined solution of QDs and ETPTCDI−CNTs was then subjected to sonication for approximately 1 h. The solution was then allowed to sit overnight in the dark. The solution was filtered over a 200 nm porous alumina membrane (Whatman Anodisc) to remove excess QDs in solution. The nanocomposite of QD−ETPTCDI−CNTs was then dispersed and diluted in a solution of DMSO to yield a concentration of 0.01% w/w of nanocomposite. The nanocomposite solution was then stored at room temperature for later use.

Fabrication of Photocurrent Response Devices. The nanocomposite solution was drop-casted onto a glass substrate (2 cm × 2 cm) while it was simultaneously heated using a hot plate. The heat from the hot plate allowed for evaporation of solvent minimizing aggregation of the nanocomposite. Two gold/palladium electrodes were sputtered onto the substrate and were spaced 150−200 μm apart. The devices were then connected to a Keithley 6487 picoammeter and placed in front of an AM1.5 solar simulator light source (Newport Inc.), where we then measured photoconductivity of the nanocomposite as the light source was shuttered on and off over a fixed period of time. The device temperature was measured using a thermocouple (type k wire probe).

Acknowledgment. We would like to acknowledge the SIU Office of Research and Development Administration (ORDA) at the Southern Illinois University at Carbondale (SIUC), National Science Foundation (NSF), and the Materials Technology Center (MTC) at SIUC for their partial financial support of this research. We also thank the IMAGE center at SIUC for allowing us to utilize their facility for performing scanning and transmission electron microscopy characterization. Hitachi High Technologies of America, Inc. is appreciated for providing us with SEM images using their SU-70 field emission scanning electron microscope

with backscatter electron detector. S. Talapatra acknowledges financial support from NSF ECCS through grant No. 0925682.

Supporting Information Available: Figures S1−S7 and their captions are available. This material is available free of charge *via* the Internet at http://pubs.acs.org.

REFERENCES AND NOTES

1. Wadia, C.; Alivisatos, A. P.; Kammen, D. M. Materials Availability Expands the Opportunity for Large-Scale Photovoltaics Deployment. *Environ. Sci. Technol.* **2009**, *43*, 2072–2077.
2. Turner, J. A. A Realizable Renewable Energy Future. *Science* **1999**, *285*, 687.
3. Whitesides, G. M.; Crabtree, G. W. Don't Forget Long-Term Fundamental Research in Energy. *Science* **2007**, *315*, 796.
4. Szuromi, P.; Jasny, B.; Clery, D.; Austin, J.; Hanson, B. *Science* **2007**, *315*, 9.
5. Lewis, N. Toward Cost-Effective Solar Energy Use. *Science* **2007**, *315*, 798.
6. Shah, A. Photovoltaic Technology: The Case for Thin-Film Solar Cells. *Science* **1999**, *285*, 692.
7. Carlson, D. E.; Wronski, C. R. Amorphous Silicon Solar Cell. *Appl. Phys. Lett.* **1976**, *28*, 11.
8. Naghavi, N.; Spiering, S.; Powalla, M.; Cavana, B.; Lincot, D. High-Efficiency Copper Indium Gallium Diselenide (CIGS) Solar Cells with Indium Sulfide Buffer Layers Deposited by Atomic Layer Chemical Vapor Deposition (ALCVD). *Prog. Photovoltaics* **2003**, *11*, 437–443.
9. O'Regan, B.; Grätzel, M. A Low-Cost, High-Efficiency Solar Cell Based on Dye-Sensitized Colloidal TiO_2 Films. *Nature* **1991**, *353*, 737–740.
10. Krebs, F. C. Polymer Photovoltaics: A Practcical Approach. *SPIE Press* **2008**, 6–7.
11. Huynh, W.; Dittmer, J.; Alivisatos, A. P. Hybrid Nanorod−Polymer Solar Cells. *Science* **2002**, *295*, 2425.
12. Huynh, W. U.; Dittmer, J. J.; William, C. L.; Whiting, G. L.; Alivisatos, A. P. Controlling the Morphology of Nanocrystal−Polymer Composites for Solar Cells. *Adv. Funct. Mater.* **2003**, *13*, 1.
13. Gur, I.; Fromer, N.; Chen, C. P.; Kanaras, A. G.; Alivisatos, A. P. Hybrid Solar Cells with Prescribed Nanoscale Morphologies Based on Hyperbranched Semiconductor Nanocrystals. *Nano Lett.* **2007**, *7*, 409–414.
14. Liu, J.; Tanaka, T.; Sivula, K.; Alivisatos, A. P.; Frechet, J. M. J. Employing End-Functional Polythiophene To Control the Morphology of Nanocrystal−Polymer Composites in Hybrid Solar Cells. *J. Am. Chem. Soc.* **2004**, *126*, 6550–6551.
15. Smith, A. M.; Shuming, N. Semiconductor Nanocrystals: Structure, Properties, and Band Gap Engineering. *Acc. Chem. Res.* **2010**, *43*, 190–200.
16. Tang, C. W. Two-Layer Organic Photovoltaic Cell. *Appl. Phys. Lett.* **1986**, *48*, 183–185.
17. Heremans, P.; Cheyns, D.; Rand, B. P. Strategies for Increasing the Efficiency of Heterojunction Organic Solar Cells: Material Selection and Device Architecture. *Acc. Chem. Res.* **2009**, *42*, 1740–1747.
18. Peet, J.; Heeger, A. J.; Bazan, G. C. "Plastic" Solar Cells: Self-Assembly of Bulk Heterojunction Nanomaterials by Spontaneous Phase Separation. *Acc. Chem. Res.* **2009**, *42*, 1700–1708.
19. Yu, G.; Hummelen, J. C.; Wudl, F.; Heeger, A. J. Polymer Photovoltaic Cells-Enhanced Efficiencies *via* a Network of Internal Donor−Acceptor Heterojunctions. *Science* **1995**, *270*, 1789–1791.
20. Brus, L. Quantum Crystallites and Nonlinear Optics. *Appl. Phys. Mater. Sci. Process.* **1991**, *53*, 465–474.
21. Murray, C. B.; Norris, D. J.; Bawendi, M. G. Synthesis and Characterization of Nearly Monodisperse CdE (E = S, Se, Te) Semiconductor Nanocrystallites. *J. Am. Chem. Soc.* **1993**, *115*, 8706–8715.
22. Iijima, S. Helical Microtubules of Graphitic Carbon. *Nature* **1991**, *354*, 56–58.
23. Baughman, R.; Zakhidov, A. A.; de Heer, W. A. Carbon Nanotubes—The Route toward Applications. *Science* **2002**, *297*, 787.
24. Eder, D. Carbon Nanotube−Inorganic Hybrids. *Chem. Rev.* **2010**, *110*, 1348–1385.
25. Hu, L.; Zhao, Y.; Ryu, K.; Zhou, C.; Stoddart, J. F.; Gruner, G. Light Induced Charge Transfer in Pyrene/CdSe-SWNT Hybrids. *Adv. Mater.* **2008**, *20*, 939–946.
26. Li, X.; Jia, Y.; Wei, J.; Zhu, H.; Wang, K.; Wu, D.; Cao, A. Solar Cells and Light Sensors Based on Nanoparticle-Grafted Carbon Nanotube Films. *ACS Nano* **2010**, *4*, 2142–2148.
27. Somani, P. R.; Somani, S. P.; Umeno, M. Application of Metal Nanoparticles Decorated Carbon Nanotubes in Photovoltaics. *Appl. Phys. Lett.* **2008**, *93*, 033315.
28. Engtrakul, C.; Kim, Y. H.; Nedeljkovic, J. M.; Ahrenkiel, S. P.; Gilbert, K. E. H.; Alleman, J. L.; Zhang, S. B.; Micic, O. I.; Nozik, A. J.; Heben, M. J. Self Assembly of Linear Arrays of Semiconductor Nanoparticles on Carbon Single-Walled Nanotubes. *J. Phys. Chem. B* **2006**, *110*, 25153–25157.
29. Juarez, B.; Klinke, C.; Kornowski, A.; Weller, H. Quantum Dot Attachment and Morphology Control by Carbon Nanotubes. *Nano Lett.* **2007**, *7*, 3564–3568.
30. Lu, C.; Akey, A.; Wang, W.; Herman, I. P. Versatile Formation of CdSe Nanoparticle−Single Walled Carbon Nanotube Hybrid Structures. *J. Am. Chem. Soc.* **2009**, *131*, 3446–3447.
31. Jeong, S.; Shim, H. C.; Kim, S.; Han, C. S. Efficient Electron Transfer in Functional Assemblies of Pyridine-Modified NQDs on SWNTs. *ACS Nano* **2010**, *4*, 324–330.
32. Peng, X.; Wong, S. S. Controlling Nanocrystal Density and Location on Carbon Nanotube Templates. *Chem. Mater.* **2009**, *21*, 682–694.
33. Landi, B. J.; Castro, S. L.; Ruf, H. J.; Evans, C. M.; Bailey, S. G.; Raffaelle, R. P. CdSe Quantum Dot−Single Wall Carbon Nanotube Complexes for Polymeric Solar Cells. *Sol. Energy Mater. Sol. Cells* **2005**, *87*, 733–746.
34. Ehli, C.; Oelsner, C.; Guldi, D.; Mateo-Alonso, A.; Prato, M.; Schmidt, C.; Backes, C.; Hauke, F.; Hirsch, A. Manipulating Single-Wall Carbon Nanotubes by Chemical Doping and Charge Transfer with Perylene Dyes. *Nat. Chem.* **2009**, *1*, 243–248.
35. Aldana, J.; Wang, Y. A.; Peng, X. Photochemical Instability of CdSe Nanocrystals Coated by Hydrophilic Thiols. *J. Am. Chem. Soc.* **2001**, *123*, 8844–8850.
36. Weaver, J.; Zakeri, R.; Aoudi, S.; Kohli, P. Synthesis and Characterization of Quantum Dot−Polymer Composites. *J. Mat. Chem.* **2009**, *19*, 3198–3206.
37. Qu, L.; Peng, A.; Peng., X. Alternative Routes toward High Quality CdSe Nanocrystals. *Nano Lett.* **2001**, *1*, 333–337.
38. Talapatra, S.; Kar, S.; Pal, S.; Vajtai, R.; Ci, L.; Victor, P.; Shaijjumon, M. M.; Kaur, S.; Nalamasu, O.; Ajayan, P. M. Direct Growth of Aligned Carbon Nanotubes on Bulk Metals. *Nat. Nanotechnol.* **2006**, *1*, 112–116.
39. Li, X.; Zhang, X.; Ci, L.; Shah, R.; Wolfe, C.; Kar, S.; Talapatra, S.; Ajayan, P. M. Air Assisted Growth of Long Aligned Carbon Nanotube Films. *Nanotechnology* **2008**, *19*, 455609.
40. Xu, B.; Xiao, X.; Yang, X.; Zang, L.; Tao, N. Large Gate Modulation in the Current of a Room Temperature Single Molecule Transistor. *J. Am. Chem. Soc.* **2005**, *127*, 2386–2387.
41. Bozzola, J. J.; Russell, L. D. *Electron Microscopy: Principles and Techniques for Biologists*; Jones and Bartlett: Boston, MA, 1992; Vol. 2, pp 225−228.
42. Pan, B.; Cui, D.; Ozkan, C. S.; Ozkan, M.; Xu, P.; Huang, T.; Liu, F.; Chen, H.; Li, Q.; He, R.; Gao, F. Effects of Carbon Nanotubes on Photoluminescence Properties of Quantum Dots. *J. Phys. Chem. C* **2008**, *112*, 939–944.
43. Dong, F.; Han, H.; Liang, J.; Lu, D. Study on the Interaction between 2-Mercaptoethanol, Dimercaprol and CdSe Quantum Dots. *Luminescence* **2008**, *23*, 321–326.
44. Wuister, S. F.; Donega, C. M.; Meijerink, A. Influence of Thiol Capping on the Exciton Luminescence and Decay Kinetics of CdTe and CdSe Quantum Dots. *J. Phys. Chem. B* **2004**, *108*, 17393–17397.
45. Van Der Meer, B. W.; Coker, G.; Chen, S. S. *Resonance*

Energy Transfer: Theory and Data; Wiley-VCH: Weinheim, Germany, 1994; pp 10−15.
46. Jakubinek, M. B.; White, M. A.; Mu, M.; Winey, K. I. Temperature Dependence of Thermal Conductivity Enhancement in Single-Walled Carbon Nanotube/Polystyrene Composites. *Appl. Phys. Lett.* **2010**, *96*, 083105.
47. Straus, D. A.; Tzolov, M.; Kuo, T. F.; Yin, A.; Xu, J. M. Photocurrent Response of the Carbon Nanotube−Silicon Heterojunction Array. *IET Circuits Dev. Syst.* **2007**, *1*, 200–204.
48. Wu, Y.; Wadia, C.; Ma, W.; Sadtler, B.; Alivisatos, A. P. Synthesis and Photovoltaic Application of Copper(I) Sulfide Nanocrystals. *Nano Lett.* **2008**, *8*, 2551–2555.
49. Furuta, A.; Kuramoto, T.; Arai, T. Additional Layer of the Multi-Walled Carbon-Nanotubes Increases the Photo-Current of a Poly(3-hexylthiophene)-Sensitized Solar Cell. *Energy Environ. Sci.* **2009**, *2*, 853–856.